NeuroImage: Clinical 33 (2022) 102900

Contents lists available at ScienceDirect

NeuroImage: Clinical

journal homepage: www.elsevier.com/locate/ynicl

Exploring brain glucose metabolic patterns in cognitively normal adults at risk of Alzheimer's disease: A cross-validation study with Chinese and ADNI cohorts

Tao-Ran Li [a,1], Qiu-Yue Dong [b,1], Xue-Yan Jiang [a,f], Gui-Xia Kang [c], Xin Li [d,e], Yun-Yan Xie [a,*], Jie-Hui Jiang [b,*], Ying Han [a,f,g,h,*], the Alzheimer's Disease Neuroimaging Initiative2

[a] Department of Neurology, Xuanwu Hospital of Capital Medical University, Beijing 100053, China
[b] Key Laboratory of Specialty Fiber Optics and Optical Access Networks, Joint International Research Laboratory of Specialty Fiber Optics and Advanced Communication, School of Information and Communication Engineering, Shanghai University, Shanghai 200444, China
[c] School of Information and Communication Engineering, Beijing University of Posts and Telecommunications, Beijing 100876, China
[d] School of Electrical Engineering, Yanshan University, Qinhuangdao 066004, China
[e] Measurement Technology and Instrumentation Key Lab of Hebei Province, Qinhuangdao 066004, China
[f] School of Biomedical Engineering, Hainan University, Haikou 570228, China
[g] Center of Alzheimer's Disease, Beijing Institute for Brain Disorders, Beijing 100053, China
[h] National Clinical Research Center for Geriatric Diseases, Beijing 100053, China

ARTICLE INFO

Keywords:
Alzheimer's disease
FDG
PET
SSM
PCA
Cognitively normal

ABSTRACT

Objective: Disease-related metabolic brain patterns have been verified for a variety of neurodegenerative diseases including Alzheimer's disease (AD). This study aimed to explore and validate the pattern derived from cognitively normal controls (NCs) in the Alzheimer's continuum.

Methods: This study was based on two cohorts; one from the Alzheimer's Disease Neuroimaging Initiative (ADNI) and the other from the Sino Longitudinal Study on Cognitive Decline (SILCODE). Each subject underwent [^{18}F] fluoro-2-deoxyglucose positron emission tomography (PET) and [^{18}F]florbetapir-PET imaging. Participants were binary-grouped based on β-amyloid (Aβ) status, and the positivity was defined as Aβ+. Voxel-based scaled subprofile model/principal component analysis (SSM/PCA) was used to generate the "at-risk AD-related metabolic pattern (ARADRP)" for NCs. The pattern expression score was obtained and compared between the groups, and receiver operating characteristic curves were drawn. Notably, we conducted cross-validation to verify the robustness and correlation analyses to explore the relationships between the score and AD-related pathological biomarkers.

Results: Forty-eight Aβ+ NCs and 48 Aβ- NCs were included in the ADNI cohort, and 25 Aβ+ NCs and 30 Aβ- NCs were included in the SILCODE cohort. The ARADRPs were identified from the combined cohorts and the two separate cohorts, characterized by relatively lower regional loadings in the posterior parts of the precuneus,

; AD, Alzheimer's disease; Aβ, β-amyloid; ^{18}F-FDG, [^{18}F]fluoro-2-deoxyglucose; PET, positron emission tomography; PCC, posterior cingulate cortex; NCs, cognitively normal controls; SSM, scaled subprofile model; PCA, principal component analysis; ARADRP, at-risk AD-related metabolic pattern; APOE, apolipoprotein E; MMSE, Mini-Mental State Examination; MoCA, Montreal Cognitive Assessment; MRI, Magnetic Resonance Imaging; AV45, [^{18}F]florbetapir; ADAS-Cog 13, Alzheimer's Disease Assessment Scale-Cognitive 13; LMT, Logical Memory Test; AVLT, Auditory Verbal Learning Test; TMT-A/B, Trail Making Test A and B; AFT, Animal Fluency Test; BNT, 30-item Boston Naming Test; MCI, Mild Cognitive Impairment; SUVR, Standardized Uptake Value Ratio; CSF, cerebrospinal fluid; PVE, partial volume effect; PCs, principal components.

* Corresponding authors at: Department of Neurology, Xuanwu Hospital of Capital Medical University, Beijing, 100053, China (Yun-Yan Xie); School of Information and Communication Engineering, Shanghai University, Shanghai, 200444, China (Jie-Hui Jiang); Department of Neurology, Xuanwu Hospital of Capital Medical University, Beijing, 100053, China (Ying Han).

E-mail addresses: litaoran1992@ccmu.edu.cn (T.-R. Li), nancy_dong@shu.edu.cn (Q.-Y. Dong), xueyanjiang1225@gmail.com (X.-Y. Jiang), 286186620@qq.com (Y.-Y. Xie), jiangjiehui@shu.edu.cn (J.-H. Jiang), hanying@xwh.ccmu.edu.cn (Y. Han).

[1] the authors contribute equally to this work.

[2] Data used in preparation of this article were obtained from the Alzheimer's Disease Neuroimaging Initiative (ADNI) database (http://adni.loni.usc.edu). As such, the investigators within the ADNI contributed to the design and implementation of ADNI and/or provided data but did not participate in analysis or writing of this report. A complete listing of ADNI investigators can be found at: http://adni.loni.usc.edu.

https://doi.org/10.1016/j.nicl.2021.102900
Received 17 June 2021; Received in revised form 17 November 2021; Accepted 24 November 2021
Available online 1 December 2021

posterior cingulate, and regions of the temporal gyrus, as well as relatively higher values in the superior/middle frontal gyrus and other areas. Patterns identified from the two separate cohorts showed some regional differences, including the temporal gyrus, basal ganglia regions, anterior parts of the precuneus, and middle cingulate. Cross-validation suggested that the pattern expression score was significantly higher in the Aβ+ group of both cohorts ($p < 0.01$), and contributed to the diagnosis of Aβ+ NCs (with area under the curve values of 0.696–0.815). The correlation analysis revealed that the score was related to tau pathology measured in cerebrospinal fluid (p-tau: $p < 0.02$; t-tau: $p < 0.03$), but not Aβ pathology assessed with [^{18}F]florbetapir-PET ($p > 0.23$).

Conclusions: ARADRP exists for NCs, and the acquired pattern expression score shows a certain ability to discriminate Aβ+ NCs from Aβ- NCs. The SSM/PCA method is expected to be helpful in the ultra-early diagnosis of AD in clinical practice.

1. Introduction

Alzheimer's disease (AD) is a progressive neurodegenerative disease with an insidious onset, which leads to a gradual decline in cognitive function, thus becoming the most common cause of dementia (Long and Holtzman, 2019). Because of the incurable and irreversible features of AD, it is of great importance to recognize AD patients at the ultra-early stage and carry out specific interventions to delay the progression of the disease (Golde et al., 2018). The advancement of biomarker detection *in vivo* has made it possible to identify AD patients in the preclinical stage (Li et al., 2021). According to the latest diagnostic frameworks (Dubois et al., 2014, 2016; Jack Jr et al., 2018), individuals exhibiting evidence of brain β-amyloid (Aβ) deposition have already entered the Alzheimer's continuum, representing a high-risk state of AD. The accurate diagnosis of cognitively healthy individuals with high brain Aβ loads (Aβ+) exactly provides an optimal therapeutic window for AD (Golde et al., 2018).

[^{18}F]fluoro-2-deoxyglucose (^{18}F-FDG) positron emission tomography (PET) imaging, in essence, measures glucose metabolism. It is a robust biomarker of neurodegeneration that is directly correlated with cognition (Jack Jr et al., 2018). Different types of dementia usually have different topological patterns of metabolism (Kato et al., 2016). For example, the glucose metabolic pattern of AD is characterized by the hypometabolism of parieto-temporal association areas, the posterior cingulate cortex (PCC), and precuneus (Gordon et al., 2018; Sakamoto et al., 2002). Importantly, recent advances have even suggested that individuals in the preclinical stage of AD may also develop regional metabolic changes (Kato et al., 2016); however, it should be noted that the available information is limited, and the results are inconsistent. Specifically, compared with cognitively normal controls (NCs) with low brain Aβ loads (Aβ-), one study found that the Aβ+ individuals had relatively increased metabolism in the lateral prefrontal cortex, lateral parietal cortex, and precuneus (Oh et al., 2014), and another study found that the enhancement was located in the superior temporal gyrus and medial thalamus (Johnson et al., 2014). Meanwhile, other studies found no differences (Dubois et al., 2018; Ewers et al., 2014; Hu et al., 2019). Moreover, when grouping the elderly according to whether their cognition will deteriorate in the future, researchers found that the progressors had reduced regional metabolism at baseline, but some results, such as PCC measurements, were also inconsistent (Stonnington et al., 2018; Toledo et al., 2014). Furthermore, the current interpretation of PET images is often made through visual inspection or by means of semiquantitative approaches that rely on the reader's expertise; however, these are prone to inter-reader disagreement (Morbelli et al., 2015), and the latter might result in an incorrect estimation of tracer binding (Lammertsma, 2017). Therefore, it is required to explore reliable and quantitative metabolic patterns to understand the brain functional changes of AD and provide new targets and ideas for the treatment of AD in the early stage.

The scaled subprofile model/principal component analysis (SSM/PCA) method is a feature extraction method that enhances the identification of significant patterns in multivariate imaging data. It is able to show the underlying relationships between brain regions that are not captured by univariate techniques and enables the assessment of network-level alterations, as opposed to treating every voxel individually (Alexander and Moeller, 1994; Eidelberg, 2009). Using this method, previous studies have identified specific metabolic patterns of healthy aging (Moeller et al., 1996), Parkinsonian syndromes (Eidelberg et al., 1994; Teune et al., 2013), and other neurodegenerative diseases (Eidelberg et al., 1995; Meles et al., 2018). In the field of AD, only a few studies have applied this method. One previous multicenter study identified an AD-related metabolic covariance pattern that was replicated in five independent samples of patients and controls; additionally, it further indicated that multivariate analysis was more sensitive and robust than univariate analysis for AD diagnosis (Habeck et al., 2008). Identical conclusions were obtained in another study where the pattern could classify patients with dementia from NCs with a sensitivity and specificity>90% (Teune et al., 2014). Other groups obtained a metabolic AD conversion-related pattern and verified that it has the potential to predict disease progression (Blazhenets et al., 2019; Katako et al., 2018). Application of this method to analyze FDG modality in the preclinical stage could help us better understand the functional changes of AD and aid in predicting disease progression. The only study on this topic enrolled patients from a single center; however, these patients were relatively older (mean: 74.1 ± 6.0 years), and the study had a small sample size (n = 52), and the authors regarded the cortical amyloid deposition as a continuous variable, therefore, no group comparisons were made (Oh et al., 2014).

The goals of this study were as follows: (1) use the SSM/PCA method to identify an "at-risk AD-related metabolic pattern (ARADRP)" by comparing the differences between Aβ+ and Aβ- NCs; (2) explore the similarities and differences of ARADRPs in two separate cohorts of Americans and Chinese; and (3) evaluate the discrimination ability of the ARADRP expression score. Notably, we performed a cross-validation of the two cohorts.

2. Participants and methods

2.1. Ethics statement

This study was approved by the Medical Ethics Committee of Xuanwu Hospital of Capital Medical University and was conducted in accordance with the Declaration of Helsinki. All subjects provided written informed consent authorizing the publication of their clinical details.

2.2. Participants

This study selected two sets of independent data from the Alzheimer's Disease Neuroimaging Initiative (ADNI, ClinicalTrials.gov identifier: NCT0123197) and the Sino Longitudinal Study on Cognitive Decline (SILCODE, ClinicalTrials.gov identifier: NCT03370744).

The ADNI was launched in 2003 and used as a public–private partnership; the related protocols can be found online (www.adni-info.org). The SILCODE project is a registered ongoing multicenter AD study on the community Han population of mainland China (Li et al., 2019). Each

subject provided detailed baseline clinical information including: sex, age, education, apolipoprotein E (APOE) status; Hachinski Ischemic Scale, Functional Activities Questionnaire, Clinical Dementia Rating scale (CDR), Mini-Mental State Examination (MMSE), and Montreal Cognitive Assessment (MoCA; basic version for SILCODE) scores; and imaging data, including T1-weighted magnetic resonance imaging (MRI), ^{18}F-FDG-PET, and [^{18}F]florbetapir (AV45)-PET. In addition, subjects from the two cohorts were also assessed for cognitive subdomains or emotional states using other scales, including the Alzheimer's Disease Assessment Scale-Cognitive 13 (ADAS-Cog 13; ADNI only), Logical Memory Test (LMT; ADNI only), Auditory Verbal Learning Test (AVLT; Rey version for ADNI, HuaShan version for SILCODE), Trail Making Test A and B (TMT-A/B), Clock Drawing Test (ADNI only), Animal Fluency Test (AFT), 30-item Boston Naming Test (BNT), Geriatric Depression Scale, Hamilton depression or anxiety scale (SILCODE only), and others.

NCs were diagnosed based on the exclusion of mild cognitive impairment (MCI) (Albert et al., 2011; Bondi et al., 2014) and dementia (McKhann et al., 1984, 2011), requiring a CDR score of 0, no obvious emotional problems, and normal education adjusted scores in the MMSE and the memory subdomain. Notably, in the SILCODE project, the diagnosis of MCI was based on neuropsychological criteria (Bondi et al., 2014). Details regarding the scales and eligibility criteria can be acquired from published protocols (Li et al., 2019) and our previous studies (Du et al., 2021; Li et al., 2020). A subset of the participants from both cohorts had subjective cognitive decline; they were analyzed together with cognitively healthy participants, which was in accordance with the research framework of the National Institute on Aging-Alzheimer's Association (Jack Jr et al., 2018). The enrolled subjects were classified as Aβ+ according to a priori principles and our previous studies that utilized an established cortical AV45 standardized uptake value ratio (SUVR) cutoff > 1.18 (Du et al., 2021; Fakhry-Darian et al., 2019; Li et al., 2020); the remaining NCs were classified as Aβ-. Finally, 48 Aβ- and 48 matched Aβ+ subjects were selected from the ADNI cohort and 30 Aβ- and 25 Aβ+ subjects were selected from the SILCODE cohort.

For the ADNI cohort, there were 21 subjects with Aβ+ NCs who underwent a second FDG-PET examination during the follow-up period, with 18 in the 24th month, two in the 48th month, and one in the 72nd month. Notably, one subject had cognitive impairment at the time of the second examination (48th month). Among the Aβ- NCs, 29 subjects underwent a second examination, with 27 in the 24th month, one in the 60th month, and one in the 72nd month; there were no subjects with cognitive impairment at that time. In addition, 42 Aβ- NCs and 45 Aβ+ NCs were tested for cerebrospinal fluid (CSF) p-tau (tau phosphorylated at the threonine 181 position) and t-tau. Details regarding the collection and tests can be acquired in the protocol and in a previous study (Shaw et al., 2009). We set the cutoff point at 23 pg/mL for p-tau in order to select subjects with fibrillar tau (T+) (Shaw et al., 2009; Zhang et al., 2020). For the SILCODE cohort, no participants underwent a second FDG-PET or CSF analysis.

2.3. PET imaging and preprocessing

For the SILCODE cohort, the imaging acquisition protocol can be acquired in the project protocol and in our previous studies (Dong et al., 2021; Du et al., 2021; Li et al., 2019). Briefly, the T1-weighted images were acquired with a magnetization-prepared rapid gradient echo sequence: field of view (FOV) = 256 × 256 mm^2, matrix = 256 × 256, slice thickness = 1 mm, gap = 0, slice number = 192, repetition time (TR) = 6.9 ms, echo time (TE) = 2.98 ms, inversion time = 450 ms, flip angle = 12°, voxel size = 1 × 1 × 1 mm^3; the PET images were acquired 40 min after intravenous injection of ^{18}F-FDG (3.7 MBq/kg) or ^{18}F-AV45 (259–370 MBq), and data were recorded using a time-of-flight ordered subset expectation maximization algorithm with the following parameters: scan duration = 35 min, eight iterations, 32 subsets matrix = 192 × 192, FOV = 350 × 350, half-width height = 3. Notably, the interval between the two PET scans was set at least three days to eliminate the effects of the first tracer. Details of the ADNI cohort are described in its protocol (www.adni-info.org).

The preprocessing steps were as follows: first, the original DICOM data were converted to the NIfTI file format using DCM2NII (https://people.cas.sc.edu/rorden/mricron/dcm2nii.html). Second, the T1-weighted images were segmented using the CAT12 toolbox (http://dbm.neuro.uni-jena.de/cat/). Third, the PET images were co-registered with their corresponding gray matter (GM) images and corrected for partial volume effect (PVE) using the PETPVE12 toolbox (http://www.fil.ion.ucl.ac.uk/spm/ext/#PETPVE12), which is based on the Muller-Gartner algorithm, in order to provide a better approximation of the true regional tracer uptake (Gonzalez-Escamilla et al., 2017). Fourth, the GM images were normalized to the Montreal Neurological Institute (MNI) standard space, and the PVE-corrected PET images were normalized to the MNI space using the forward transformation parameters determined by the GM image spatial normalization. Finally, an 8-mm full width at half-maximum (FWHM) Gaussian kernel was used to smooth the images. Notably, we also performed preprocessing without PVE correction in parallel. All procedures were implemented using the Statistical Parametric Mapping (SPM8) software (www.fil.ion.ac.uk/spm). For amyloid-PET, with reference to our previous studies (Dong et al., 2021; Du et al., 2021; Li et al., 2020), the whole cerebellum was used as the reference region and the whole cerebral cortex was used as the region of interest (ROI) to calculate the SUVR.

2.4. Identification and cross-validation of the ARADRPs

Pattern analysis was performed using the ScanVP 7.0w package (http://www.feinsteinneuroscience.org) and implemented in MATLAB R2018a (MathWorks, Natick, MA, United States), as previously described (Alexander and Moeller, 1994; Eidelberg, 2009; Spetsieris et al., 2007; Spetsieris and Eidelberg, 2011). A 35% threshold of the whole-brain intensity maximum was applied to remove out-of-brain voxels, which resulted in a mask of mainly gray matter, followed by a logarithmic transformation of the mean glucose metabolism within each voxel for each subject. After removing the between-subject and between-region averages, PCA was applied. The singular value decomposition of the covariance matrix results in a set of independent and orthogonal principal components (PCs), and the PCs explaining the top 50% variance were selected for further analysis. ARADRP was determined from a linear combination of the selected PCs with the lowest Akaike information criterion (AIC) value in a stepwise logistic regression procedure (Akaike, 1994). We regressed covariates including age, sex, education, and APOE ε4 status during the process. The generated covariance pattern was converted to a z-score map standardized by the standard deviation, consisting of covarying regions of increased and decreased weights relative to the mean and relating them to each other. Voxels with z-scores threshold of $z \geq |1.65|$ ($p \leq 0.05$) were visually examined, and the cluster level was set above 30. Finally, the subject expression scores were computed using the topographic profile rating algorithm. The mathematical formulations used in the above process can be obtained from the above references.

In this study, the pattern reliability was estimated at each voxel using a bootstrapping method of 1000 iterations (Habeck et al., 2008; Oh et al., 2014). We calculated three ARADRPs. The first pattern was obtained from the combined cohorts (PCs 2, 4, 5, 7, 8, 10 and 11), and the other two patterns were from the independent cohort (PCs 1, 3, 6, 7, 8, 9 and 11 for the ADNI-derived, PCs 1, 2, 5 and 6 for the SILCODE-derived). To verify the consistency of the ARADRPs, the pattern trained from one cohort (as a training set) was verified in the other cohort (as a test set). Details regarding the proportion and coefficient of each PC, as well as the test results using only the two PCs with the highest proportion, are presented in the Supplementary Material.

2.5. Regional metabolism of the medial temporal lobe and voxel analysis

The medial temporal lobe is a typical region where the metabolism decreases early (Knopman et al., 2013); it is also a typical hypometabolic region of MCI and AD (Kato et al., 2016; Landau et al., 2011). We obtained the FDG SUVR of the medial temporal lobe using the same method as that used in previous research (Knopman et al., 2013). Furthermore, a voxel-wise two-sample *t*-test was performed between the Aβ+ and Aβ- groups with sex, age, education, APOE ε4 status, and the gray matter probability maps as covariates. The analysis was performed using SPM in accordance with our previous study (Dong et al., 2021). After obtaining the above mask, we further quantified the voxel-wise SPM pattern by dividing the mask-derived value by the cerebral cortex-derived value.

2.6. Statistical analysis

The demographic and neuropsychological data were summarized as numbers (%) or as means ± standard deviations for categorical and continuous variables, respectively. Chi-square tests were used for categorical variables, and independent two-sample t-tests were used for continuous variables.

A two-sample *t*-test was used to analyze the statistical differences in the pattern expression scores between the Aβ+ and Aβ- groups and between the T+ and T- groups. The area under the curve (AUC) values of the receiver operating characteristic (ROC) curves were used to evaluate the ability of the indicators to distinguish Aβ+ NCs from Aβ- NCs. In order to clarify whether there is a certain similarity between the patterns (ADNI-derived and SILCODE-derived) and the pattern stability over time, we performed a Pearson correlation analysis on the scores. Stability was also verified in a paired two-sample *t*-test. Furthermore, we explored the correlations between the pattern expression scores and the pathological biomarkers (global AV45 SUVR, CSF p-tau, and t-tau) using a linear regression model adjusted for sex, age, education, and APOE ε4 status. The significance threshold was set at $p < 0.05$, and the above analyses were performed using SPSS v24 (SPSS Inc., Chicago, IL, United States).

3. Results

3.1. Subject characteristics

Detailed information on the two cohorts can be found in Table 1. In the ADNI cohort, 48 Aβ- and 48 Aβ+ NCs were included; the latter group showed a higher proportion of APOE ε4 carriers ($p < 0.005$) and slightly worse performance scores on the neuropsychological tests, including the LMT, ADAS-Cog 13, AVLT-delayed recall, AFT and BNT tests ($p < 0.05$). There were no differences in age, sex ratio, education, and scores on the different scales, including the AVLT-recognition, TMT-A/B, MMSE, and MoCA scales, between the two groups. In the SILCODE cohort, 30 Aβ- and 25 Aβ+ NCs were included; the latter showed a higher proportion of women ($p < 0.05$), and there were no differences in other information. As expected, individuals in the Aβ+ group showed a higher AV45 SUVR ($p < 0.001$), CSF p-tau ($p < 0.005$), and t-tau ($p < 0.05$) compared to the Aβ- group. It should be noted that the average age and education levels of individuals in the ADNI cohort were both significantly higher than those in the SILCODE cohort.

3.1.1. ARADRP of the combined cohorts and the two cohorts

When the two cohorts were combined, the regional loadings were relatively decreased in the PCC, inferior parietal lobules, insula, calcarine, lingual gyrus, and posterior parts of the precuneus; they were also relatively increased in the precentral gyrus, middle cingulate gyrus, middle and inferior frontal gyrus, and in anterior parts of the precuneus (Fig. 1A). In addition, there were mixed changes in weight in areas including the cerebellum, cuneus, basal ganglia regions, fusiform gyrus, and in scattered areas of the middle occipital gyrus and the middle and inferior temporal gyrus.

As shown in Fig. 2A and Fig. 3A, we subsequently analyzed the two cohorts independently and obtained two different patterns that revealed highly similar topographic features. Specifically, the regional loadings were relatively decreased in the cerebellum, PCC, and posterior parts of the precuneus, increased in the superior/middle frontal gyrus and precentral gyrus, and mixed in the inferior parietal lobules, cuneus, fusiform gyrus, calcarine and lingual gyrus, in both cohorts. In terms of differences, the ARADRP of the ADNI cohort showed a deeper and wider decreased regional loading in the middle/inferior temporal gyrus compared to the SILCODE cohort. The increased regional loadings in the middle cingulate and the decreases in the basal ganglia regions identified in the ADNI cohort could not be observed in the SILCODE cohort. Similarly, the relatively decreased regional loadings in the anterior parts

Table 1
Clinical characteristics of participants.

	ADNI (n = 96)		SILCODE (n = 55)	
	Aβ- (n = 48)	Aβ+ (n = 48)	Aβ- (n = 30)	Aβ+ (n = 25)
Female (n%)	28 (58%)	32 (67%)	15 (50%)	20 (80%)*
Age	75.07 ± 5.67	75.19 ± 5.98	66.23 ± 4.71§	66.32 ± 4.91†
Education	17.06 ± 2.21	16.00 ± 2.72	13.13 ± 3.07§	12.76 ± 3.06†
APOE ε4 carries (n%)	8 (17%)	22 (46%)**	9 (30%)	8 (32%)
FAQ	0.25 ± 0.89	0.35 ± 0.79	0.23 ± 0.68	0.44 ± 0.96
LMT	14.02 ± 3.06	12.52 ± 3.02*	NA	NA
ADAS-Cog 13	8.00 ± 3.28	9.60 ± 4.10*	NA	NA
AVLT-delayed recall	8.67 ± 3.67	6.88 ± 3.39*	7.63 ± 2.48	7.68 ± 1.93
AVLT-recognition	13.31 ± 1.73	12.81 ± 2.19	22.57 ± 1.57	22.48 ± 1.29
TMT-A	31.17 ± 8.69	34.81 ± 10.48	58.80 ± 15.83	54.08 ± 19.12
TMT-B	83.94 ± 48.01	91.69 ± 39.94	128.33 ± 28.13	129.72 ± 33.28
AFT	21.94 ± 5.71	19.69 ± 5.19*	19.37 ± 5.49	20.20 ± 5.22
BNT	28.92 ± 1.09	27.81 ± 2.12*	25.77 ± 3.04	25.92 ± 2.94
MMSE	29.31 ± 1.27	29.19 ± 0.79	28.83 ± 1.29	28.88 ± 2.08
MoCA	25.94 ± 2.58	25.29 ± 2.35	26.03 ± 2.13	26.68 ± 2.12
CSF t-tau (pg/ml)	239.24 ± 94.06 (42Ava)	287.99 ± 108.57 (45Ava)*	NA	NA
CSF p-tau (pg/ml)	21.24 ± 8.95 (42Ava)	28.36 ± 11.98 (45Ava)**	NA	NA
AV45 SUVR	1.02 ± 0.05	1.37 ± 0.17***	1.10 ± 0.05	1.23 ± 0.06***

Categorical and continuous measures are presented as numbers (%) or means ± standard deviations. Statistical analyses were conducted using chi-square tests for categorical variables and independent two-sample t-tests. Comparisons between Aβ- and Aβ+, * $p < 0.05$, ** $p < 0.005$, *** $p < 0.001$. Comparisons between the same groups of the two cohorts, § (Aβ-) means $p < 0.001$, † (Aβ+) means $p < 0.001$; the comparisons were not performed using neuropsychological scales, except for the MMSE, due to differences in versions and cultural backgrounds. The AVLT scale used in the ADNI cohort was the Rey version, while that used in the SILCODE cohort was the HuaShan version; the MoCA scale used in the SILCODE cohort was the MoCA-Basic version. Abbreviations: ADNI, Alzheimer's Disease Neuroimaging Initiative; SILCODE, Sino Longitudinal Study on Cognitive Decline; Aβ, β-amyloid; APOE, apolipoprotein E; FAQ, Functional Activities Questionnaire; LMT, Logical Memory Test; ADAS-Cog 13, Alzheimer's Disease Assessment Scale-Cognitive 13; AVLT, Auditory Verbal Learning Test; TMT, Trails Making Test; AFT, Animal Fluency Test; BNT, Boston Naming Test; MMSE, mini-mental state examination; MoCA, Montreal cognitive assessment; AV45, [^{18}F]florbetapir; SUVR, standardized uptake value ratio; CSF, cerebrospinal fluid; p-tau, phosphorylated tau; Ava, available; NA, not available.

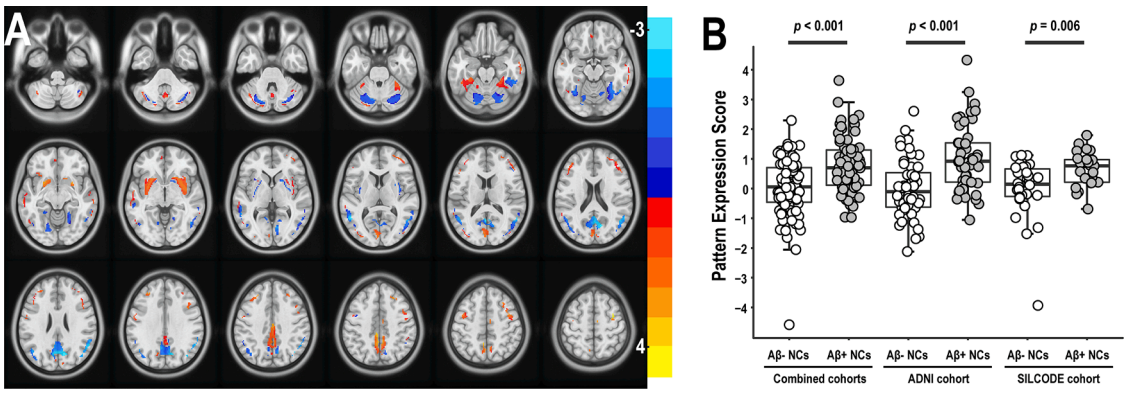

Fig. 1. ARADRP identified by spatial covariance analysis of [^{18}F]-FDG-PET scans from Aβ+ NCs and Aβ- NCs in the combined cohorts. (**A**) Abnormal metabolic covariance topography in the ARADRP of the combined cohorts showing negative (cold color) and positive (warm color) regions coded by Z-scores. (**B**) Individual pattern expression score of the Aβ+ NCs and the Aβ- NCs using the ARADRP identified from the combined cohorts. It should be noted that the scores are not absolute values, and the reference values used in the z-scoring are different between the combined cohorts and the independent cohort. Abbreviations: ADNI, Alzheimer's Disease Neuroimaging Initiative; SILCODE, Sino Longitudinal Study on Cognitive Decline; Aβ, β-amyloid; NCs, cognitively normal controls; ARADRP, at-risk Alzheimer's disease-related metabolic pattern; [^{18}F]-FDG-PET, [^{18}F]fluoro-2-deoxyglucose positron emission tomography.

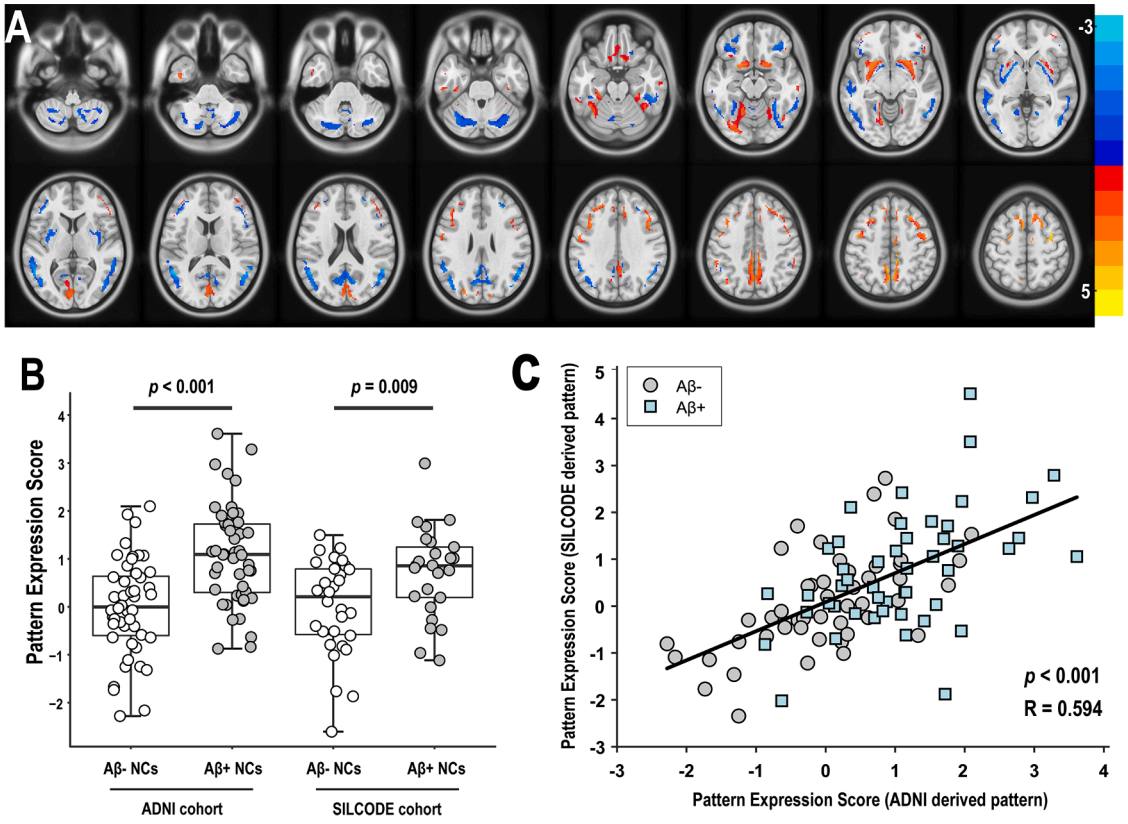

Fig. 2. ARADRP identified by spatial covariance analysis of [^{18}F]-FDG-PET scans from Aβ+ NCs and Aβ- NCs in the ADNI cohort. (**A**) Abnormal metabolic covariance topography in ARADRP of the ADNI cohort showing negative (cold color) and positive (warm color) regions coded by Z-scores. (**B**) Individual pattern expression score of the Aβ+ NCs and the Aβ- NCs using the ARADRP identified from the ADNI cohort; the SILCODE cohort was used for validation. (**C**) Correlation analysis of the pattern expression score among individuals in the ADNI cohort; the patterns were derived from the ADNI and the SILCODE cohorts. Abbreviations: ADNI, Alzheimer's Disease Neuroimaging Initiative; SILCODE, Sino Longitudinal Study on Cognitive Decline; Aβ, β-amyloid; NCs, cognitively normal controls; ARADRP, at-risk Alzheimer's disease-related metabolic pattern; [^{18}F]-FDG-PET, [^{18}F]fluoro-2-deoxyglucose positron emission tomography.

of the precuneus and the increases in the superior temporal gyrus identified in the SILCODE cohort could not be observed in the ADNI cohort. Furthermore, the scores obtained using different patterns showed significant and positive correlations in both the ADNI cohort ($R = 0.594$, $p < 0.001$; Fig. 2C) and the SILCODE cohort ($R = 0.615$, $p < 0.001$; Fig. 3C).

We emphasize that these are relative changes of weights, not absolute quantifications.

3.1.2. *Cross-validation of the ARADRPs between the ADNI and SILCODE cohorts*

The two-sample t-tests revealed significant differences in ARADRP expression scores between the Aβ+ and Aβ- groups in both cohorts. As shown in Fig. 1B, the average score of the Aβ+ group was significantly

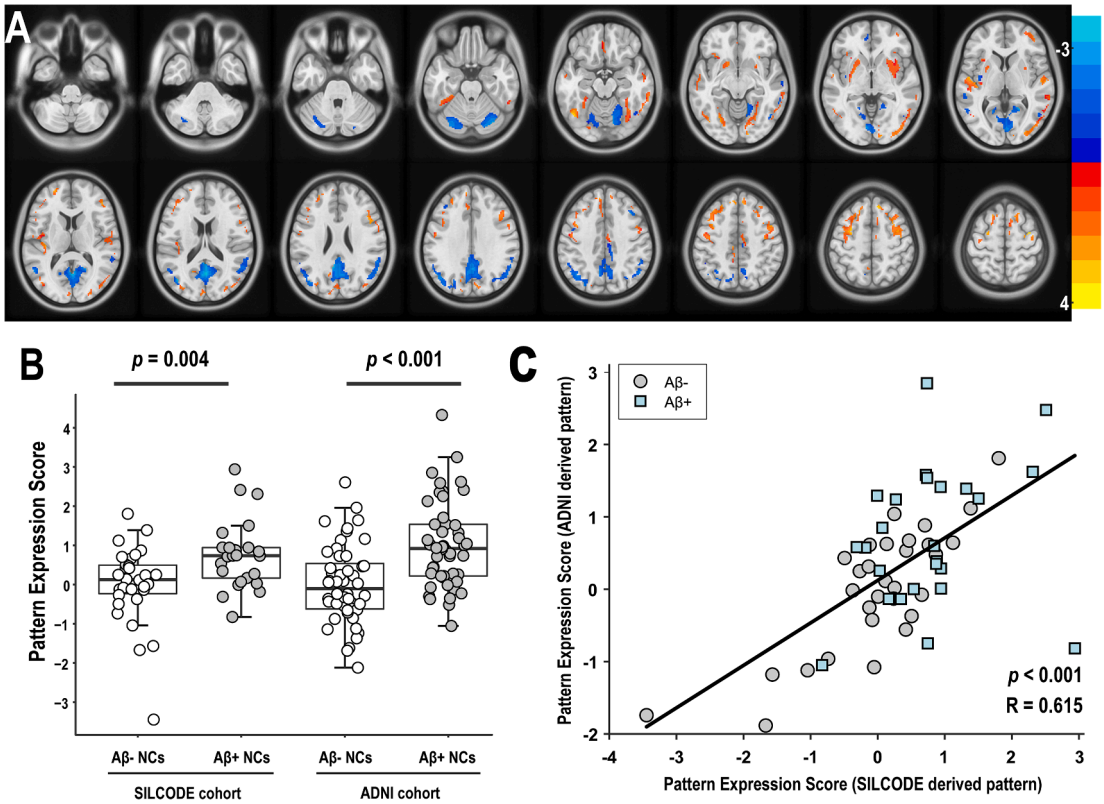

Fig. 3. ARADRP identified by spatial covariance analysis of [^{18}F]-FDG-PET scans from Aβ+ NCs and Aβ- NCs in the SILCODE cohort. (**A**) Abnormal metabolic covariance topography of the ARADRP from the SILCODE cohort showing negative (cold color) and positive (warm color) regions coded by Z-scores. (**B**) Individual pattern expression score of the Aβ+ NCs and the Aβ- NCs using the ARADRP identified from the SILCODE cohort; the ADNI cohort was used for validation (right). (**C**) Correlation analysis of the pattern expression scores among individuals in the SILCODE cohort; the patterns were derived from the ADNI and the SILCODE cohorts. Abbreviations: ADNI, Alzheimer's Disease Neuroimaging Initiative, SILCODE, Sino Longitudinal Study on Cognitive Decline Aβ, β-amyloid NCs, cognitively normal controls ARADRP, at-risk Alzheimer's disease-related metabolic pattern [18F]-FDG-PET, [18F]fluoro-2-deoxyglucose positron emission tomography.

higher than that of the Aβ- group in the combined cohort ($p < 0.001$), the ADNI cohort ($p < 0.001$), and the SILCODE cohort ($p = 0.006$), and the pattern was identified in the combined cohorts. When analyzing the two cohorts separately, the average score was also different between the two groups. Specifically, Fig. 2B shows that the score of the Aβ+ group was significantly higher than that of the Aβ- group, both in the training set (ADNI; $p < 0.001$) and the test set (SILCODE; $p = 0.009$), and that this pattern was identified from the ADNI cohort. Fig. 3B shows similar results both in the training set (SILCODE; $p = 0.004$) and the test set (ADNI; $p < 0.001$), and the pattern was identified from the SILCODE cohort.

Notably, we also acquired patterns without regression of the covariates. We can clearly see that the patterns derived from a single cohort were not significantly affected by regression effects, while the pattern derived from the combined cohorts was affected (Supplementary Fig. 1). Cross-validation also indicated differences between the groups in both the training and test sets (Supplementary Table 1).

3.1.3. ROC analysis

As shown in Table 2, when distinguishing Aβ+ NCs from Aβ- NCs, indicators including the pattern expression scores, the typical scales, the combination of these scores and scales, the voxel-wise SPM expression scores, and the regional metabolism of the medial temporal lobe were compared using ROC analysis in both cohorts. As expected, since the Aβ+ NCs had not yet developed cognitive impairment, the overall cognitive function evaluated by the MMSE scale or the MoCA scale could not distinguish between the two groups, with AUCs of 0.591 and 0.593 respectively in the SILCODE cohort and 0.603 and 0.580 respectively in the ADNI cohort. Comparatively, the average distinguishing ability of the pattern expression score reached 0.815 and 0.696 in the training set (ADNI) and test set (SILCODE), respectively, in the model trained by the ADNI cohort, and reached 0.745 and 0.700 in the training set (SILCODE) and test set (ADNI), respectively, in the model trained by the SILCODE cohort. When the scores and scales (MMSE and MoCA) were combined, the distinguishing ability was not significantly improved. Using the pattern obtained from the combined cohorts, the average distinguishing ability was 0.729 for the ADNI cohort and 0.739 for the SILCODE cohort, and this value did not improve when combining the scores and scales together. In addition, we found that the voxel-wise SPM expression score and the FDG SUVR of the medial temporal lobe performed poorly when distinguishing the groups in our two cohorts, with AUCs between 0.513 and 0.667. The details can be found in Table 2, and the voxel-wise SPM topographical results are presented in Supplementary Fig. 3.

The results with no PVE correction preprocessing are summarized in the Supplementary material (Table 2 and Fig. 2); the performance was not as good as with the PVE correction.

3.1.4. Relationships with biomarkers and follow-up analysis

Using the pattern obtained from the combined cohorts, the pattern expression score was not correlated with the AV45 SUVR ($R = 0.148$, $p = 0.333$; Fig. 4A); however, it was significantly and negatively correlated with CSF p-tau ($R = -0.446$, $p = 0.003$; Fig. 4B) and t-tau ($R = -0.406$, $p = 0.007$; Fig. 4C), in the Aβ+ NCs of the ADNI cohort. Correspondingly, the A+T+ group showed a decreasing trend compared to the A+T- group ($p = 0.088$; Supplementary Fig. 4). Identical conclusions were also obtained using the ADNI- or SILCODE-derived pattern (A+T+ vs. A+T-: $p = 0.058$ and 0.163, respectively; correlation with AV45 SUVR: $p = 0.237$ and 0.545, respectively; with p-tau: $p = 0.005$ and

Table 2
ROC curves.

Categorical variables	ADNIAUCs (95% CI)	SILCODEAUCs (95% CI)
Pattern trained by itself	0.815 (0.730–0.899)	0.745 (0.615–0.876)
Pattern trained by the other	0.700 (0.596–0.805)	0.696 (0.615–0.836)
MMSE	0.603 (0.488–0.718)	0.591 (0.437–0.744)
MoCA	0.580 (0.466–0.695)	0.593 (0.440–0.746)
Pattern (itself) + MMSE + MoCA	0.824 (0.743–0.905)	0.784 (0.662–0.906)
Pattern (the other) + MMSE + MoCA	0.706 (0.601–0.811)	0.732 (0.600–0.864)
Pattern trained by the two cohorts	0.729 (0.629–0.830)	0.739 (0.608–0.869)
Pattern (two cohorts) + MMSE + MoCA	0.748 (0.650–0.846)	0.745 (0.614–0.877)
FDG SUVR of the medial temporal lobe	0.578 (0.463–0.693)	0.528 (0.370–0.686)
Voxel-wise SPM pattern (itself)	0.667 (0.558–0.776)	0.513 (0.358–0.668)
Voxel-wise SPM pattern (the other)	0.560 (0.445–0.676)	0.617 (0.468–0.767)
Voxel-wise SPM pattern (two cohorts)	0.657 (0.547–0.766)	0.571 (0.419–0.723)

ROC curves were used to distinguish Aβ+ NCs from Aβ- NCs in the two cohorts. In the ADNI (SILCODE) cohort, the pattern trained by 'itself' indicates that the pattern was acquired from the ADNI (SILCODE) cohort, and the pattern trained by 'the other' indicates that the pattern was acquired from the SILCODE (ADNI) cohort. The pattern trained by the 'two cohorts' indicates that the pattern was acquired from the combined two cohorts. Abbreviations: AUCs, areas under the curve; ROC, receiver operating characteristic; ADNI, Alzheimer's Disease Neuroimaging Initiative; SILCODE, Sino Longitudinal Study on Cognitive Decline; CI, confidence interval; Aβ, β-amyloid; NCs, cognitively normal controls; MMSE, Mini-Mental State Examination; MoCA, Montreal Cognitive Assessment; FDG, fluoro-2-deoxyglucose; SUVR, standardized uptake value ratio.

0.014, respectively; with t-tau: $p = 0.005$ and 0.027, respectively; Supplementary Figure 4 and 5). However, there was no relationship between the scores and tau markers in the Aβ- NCs or in all of the individuals (Aβ- NCs: p-tau, R = -0.160 to 0.187, $p = 0.249$ to 0.709; t-tau, R = -0.187 to 0.188, $p = 0.244$ to 0.747. All individuals: p-tau, R = -0.056 to −0.016, $p = 0.609$ to 0.884; t-tau, R = -0.112 to −0.017, $p = 0.309$ to 0.878. Data not shown). Details regarding the biomarker levels of participants with different diagnostic profiles as well as the relationships between the AV45 SUVRs and pattern expression scores are reported in the Supplementary Material.

Among cognitively stable individuals with follow-up data, the paired two-sample *t*-test indicated that the pattern expression score remained unchanged over time ($p = 0.7629$ of the Aβ- NCs, $p = 0.7473$ of the Aβ+ NCs), and the scores acquired at the two different time points were significantly correlated (Aβ- NCs: R = 0.9143, $p < 0.0001$; Aβ+ NCs: R = 0.6836, $p = 0.0009$). Only one Aβ+ subject had developed cognitive impairment that was evident on the second FDG-PET examination, and her score increased from −0.06 to 0.67. The results are shown in Supplementary Figure 6 and 7.

4. Discussion

In this study, we used a voxel-based SSM/PCA method to analyze FDG-PET images and identified the metabolic patterns of NCs in the Alzheimer's continuum. Specifically, we constructed ARADRPs for Americans from the ADNI cohort and for the Chinese from the SILCODE cohort, explored their differences and similarities, and conducted cross-validation. Furthermore, we found that the pattern expression scores contributed to the identification of Aβ+ NCs among cognitively healthy individuals, to a certain extent. Notably, the ARADRPs identified from one cohort could be applied to the other cohort, and vice versa, and the scores were stable over time, indicating that the SSM/PCA can be reliably used to obtain the ARADRPs from FDG-PET images, and the extracted patterns have the potential to diagnose Aβ+ NCs.

The disease-related metabolic covariance patterns identified from the combined cohorts or the two separate cohorts were all characterized by relatively lower regional loadings in the posterior parts of the precuneus, PCC, and parts of the temporal gyrus, results that are in line with previous reports that specialized in AD or MCI (Blazhenets et al., 2019; Habeck et al., 2008; Mattis et al., 2016; Meles et al., 2017; Teune et al., 2014). These results indicate that NCs in the Alzheimer's continuum have already developed regional changes in weights, which likely represent metabolic abnormalities; these limited damages are likely to worsen as the disease progresses, gradually involving parieto-temporal cortices and frontal association areas in the advanced stages (Gordon et al., 2018; Kato et al., 2016). The cerebellum is generally believed to be immune to AD damage; however, some studies have found that its regional loadings are relatively increased in AD patients (Blazhenets et al., 2019; Meles et al., 2017; Teune et al., 2014), and even in Aβ+ NCs (Oh et al., 2014). Inconsistently, in our study, we found that regional loadings in the cerebellum were mainly decreased, and the current evidence is insufficient to provide a clear explanation regarding the cause of this. In addition, the regional loadings of other regions, including the basal ganglia regions, inferior parietal cortex, and others, were relatively increased; these regions have also been reported in previous AD-related studies (Blazhenets et al., 2019; Habeck et al., 2008; Oh et al., 2014). A relatively higher metabolism is usually interpreted as a compensatory mechanism for which to maintain normal cognitive functions in the face of insults caused by Aβ deposition (Kadir et al., 2012). It should also be noted that the absolute metabolism of these regions may actually be decreased or unchanged, even though they appeared to have elevated weights in comparison to other areas involved in this pattern (Eidelberg et al., 1994, 1995). The ARADRPs obtained from the two separate cohorts indeed have some

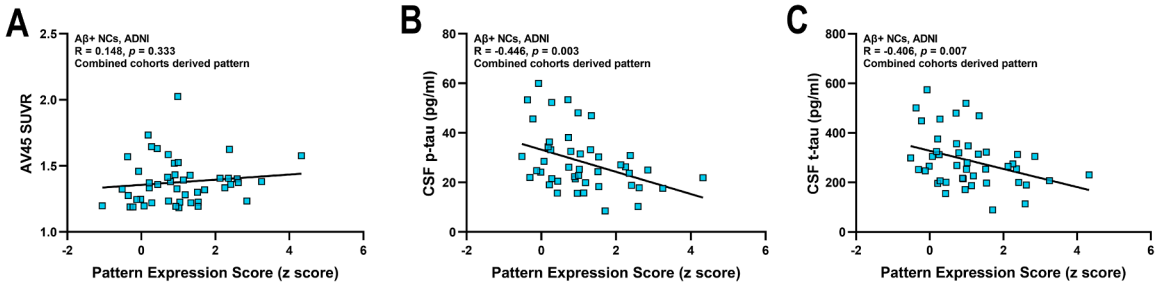

Fig. 4. Correlation analysis between the pattern expression scores and the pathological biomarkers. The ARADRP was identified from the combined two cohorts and a correlation analysis was performed between the pattern expression scores and the AV45 SUVRs (**A**), CSF p-tau levels (**B**), and CSF t-tau levels (**C**) in the ADNI cohort. Abbreviations: AV45, [^{18}F]florbetapir; SUVR, standardized uptake value ratio; Aβ, β-amyloid; NCs, cognitively normal controls; ARADRP, at-risk Alzheimer's disease-related metabolic pattern; ADNI, Alzheimer's Disease Neuroimaging Initiative; CSF, cerebrospinal fluid; p-tau, phosphorylated tau.

inconsistencies, which may be caused by factors including the relatively older age of the ADNI cohort and APOE ε4 status mismatches between the groups of the ADNI cohort. More specifically, the average age of individuals in the ADNI cohort was approximately ten years greater than the individuals in the SILCODE cohort, and normal aging was accompanied by decreased metabolism in the temporal and parietal regions (Shen et al., 2012), which may result in a serious weight reduction in the temporal lobes of individuals in the ADNI cohort. Furthermore, aging is associated with specific metabolic covariation profiles (Moeller et al., 1996). As an independent risk factor for AD (Long and Holtzman, 2019), previous studies have uncovered the negative effects of APOE ε4 on metabolism in the elderly (Kato et al., 2016; Seo et al., 2016; Stonnington et al., 2020); thus, the higher carrying rate of APOE ε4 in the Aβ+ group of the ADNI cohort likely leads to an increase in glucose consumption (Seo et al., 2016). Interestingly, the extent and degree of the decreased weights in the precuneus regions of the SILCODE cohort were more severe than in the ADNI cohort. This may be partially consistent with our previous findings that the high-risk individuals of AD in the SILCODE cohort have already developed functional dysfunctions in the precuneus region (Yang et al., 2018). In addition, it is undeniable that the differences in imaging protocols, systems, and reconstruction algorithms, as well as differences in race and cultural backgrounds, may also lead to inconsistencies. However, in general, ARADRPs still show good consistency.

According to the "amyloid cascade hypothesis" or real-world studies (Long and Holtzman, 2019; Luo et al., 2020), intracranial Aβ deposition is the initial pathological change observed in AD. In addition to amyloid-PET and CSF detection, current studies have mainly focused on circulating Aβ in the preclinical stage of AD; however, they have obtained inconsistent conclusions (Li et al., 2021). A series of recent studies have suggested that the peripheral p-tau181 and 217 have great potential in identifying Aβ+ NCs, and that the accuracy has reached as incredibly high score of 0.70–0.90 (Li et al., 2021). However, the detection of peripheral blood biomarkers is complicated, easily affected by a variety of interference factors, and relies on precision equipment (Verberk et al., 2020). Here, we found that the pattern expression score showed a certain ability to identify Aβ+ NCs. More specifically, the Aβ+ NCs showed higher scores than the Aβ- subjects ($p < 0.01$). The ROC analysis showed that the average AUCs were 0.745 and 0.815 in the training set and 0.696 and 0.700, respectively, in the test set. Although the discrimination ability was not as outstanding compared to the CSF and blood-based biomarkers of Aβ or tau, the results were considered reasonable considering that large-scale neurodegeneration had not yet occurred at this stage. After all, the neurodegeneration reflected by FDG-PET is just a downstream event. Identical to previous studies (Baker et al., 2017; Wolfsgruber et al., 2020), the scores of some fine neuropsychological examinations differ between groups (ADNI only); however, this was only evident at the group level, and the actual values were low (Li et al., 2021). Comparatively, the SSM/PCA method improved the accuracy. From another perspective, FDG-PET is more popular and has been widely used in clinical diagnosis. Further analysis suggested that the pattern expression score was not correlated with brain Aβ deposition, rather it was negatively and significantly correlated with CSF tau biomarkers among NCs who in the Alzheimer's continuum. The negative correlation observed was unexpected and showed that the higher the score, the less serious the tau pathology. From our perspectives, this may be a compensatory mechanism in the ultra-early stage of the Alzheimer's continuum, which was also observed in functional MRI studies performed by our group and other researchers (Chen et al., 2020; Skouras et al., 2019; Sun et al., 2016); further verification is still needed. We believe these results echo previous reports to some extent, showing that the reduction in glucose metabolism in AD-sensitive areas is not directly related to Aβ deposition (Besson et al., 2015; Jagust and Landau, 2012). Other evidence has suggested that elevated brain Aβ deposition alone is likely insufficient to produce neuronal damage and cognitive changes (Aschenbrenner et al., 2018); the correlation between Aβ and metabolism is likely to be mediated by neurofibrillary tangles with a temporal delay (Besson et al., 2015). No biomarkers will fit all needs; the ARADRP confirmed here was stable over time and can be used to identify Aβ+ NCs to a certain extent. It is likely to be used as an auxiliary biomarker and to predict future cognitive deterioration.

Several limitations were present in this study: (1) The small sample size limited the statistical power of our data. We tried to overcome this issue, but the requirement of simultaneous amyloid-PET and FDG-PET greatly limited the number of potential participants. (2) In order to match the age of the ADNI cohort, we adopted a stratified sampling method, which might have caused some uncertainty. (3) Our study was mainly cross-sectional, and longitudinal follow-up data with more conversion subjects might be needed to further support our results. (4) The follow-up analysis showed that the pattern expression scores of some cognitively stable subjects changed greatly, and the changing amplitude was even greater than that of the only cognitively unstable subject; this is difficult to explain and may be due to a bias, suggesting that the current patterns need to be further improved in the future. (5) Other factors such as gene polymorphisms, diet styles, and levels of physical activity may also influence brain metabolism (Berti et al., 2018; Matthews et al., 2014; Stonnington et al., 2020); however, these factors were not considered in this study. Considering the shortcomings of our research and the limitations in this field, a multicenter collaboration that includes more subjects is required to verify the robustness of the results and the possibility of the pattern as a biomarker.

5. Conclusion

Our study suggests that a certain degree of metabolic changes had already occurred in the NCs in the Alzheimer's continuum; in addition, the ARADRP identified by the SSM/PCA method exists. Furthermore, compared with the traditional semiquantitative identification method that utilizes FDG and neuropsychological scales, the acquired pattern expression score showed a certain ability to discriminate Aβ+ NCs from Aβ- NCs. The SSM/PCA method is expected to be helpful in the ultra-early diagnosis of AD in clinical practice.

CRediT authorship contribution statement

Tao-Ran Li: Data curation, Formal analysis, Investigation, Methodology, Writing – original draft, Writing – review & editing. **Qiu-Yue Dong:** Data curation, Formal analysis, Investigation, Methodology, Writing – original draft, Writing – review & editing. **Xue-Yan Jiang:** Conceptualization, Methodology, Writing – review & editing. **Gui-Xia Kang:** Data curation, Writing – review & editing. **Xin Li:** Data curation, Writing – review & editing. **Yun-Yan Xie:** Project administration, Supervision, Funding acquisition, Resources, Investigation. **Jie-Hui Jiang:** Conceptualization, Formal analysis, Methodology, Project administration, Supervision, Writing – original draft, Writing – review & editing. **Ying Han:** Conceptualization, Funding acquisition, Project administration, Supervision, Writing – review & editing.

Acknowledgments

The authors wish to thank Bi-Xiao Cui and Jie Lu (Department of Nuclear Medicine, Xuanwu Hospital Capital Medical University, Beijing, China), for their help in the identification of individuals who in the Alzheimer's continuum.

Data availability statement

The data that support the findings of this study are available from the corresponding author upon reasonable request.

Funding information

This work was supported by grants from the National Key Research and Development Program of China (2016YFC1306300, 2018YFC1312001), the National Natural Science Foundation of China (61633018, 82020108013), and the Shanghai Health Commission (2020YJZX0111).

Appendix A. Supplementary data

Supplementary data to this article can be found online at https://doi.org/10.1016/j.nicl.2021.102900.

References

Akaike, H., 1994. A new look at statistical model identification. IEEE Trans. Autom. Control 19, 716–723. https://doi.org/10.1109/tac.1974.1100705.

Albert, M.S., DeKosky, S.T., Dickson, D., Dubois, B., Feldman, H.H., Fox, N.C., Gamst, A., Holtzman, D.M., Jagust, W.J., Petersen, R.C., Snyder, P.J., Carrillo, M.C., Thies, B., Phelps, C.H., 2011. The diagnosis of mild cognitive impairment due to Alzheimer's disease: recommendations from the National Institute on Aging-Alzheimer's Association workgroups on diagnostic guidelines for Alzheimer's disease. Alzheimers & Dementia 7 (3), 270–279. https://doi.org/10.1016/j.jalz.2011.03.008.

Alexander, G.E., Moeller, J.R., 1994. Application of the scaled subprofile model to functional imaging in neuropsychiatric disorders: A principal component approach to modeling brain function in disease. 2, 79-94. https://doi.org/10.1002/hbm.460020108.

Aschenbrenner, A.J., Gordon, B.A., Benzinger, T.L.S., Morris, J.C., Hassenstab, J.J., 2018. Influence of tau PET, amyloid PET, and hippocampal volume on cognition in Alzheimer disease. Neurology 91 (9), e859–e866.

Baker, J.E., Lim, Y.Y., Pietrzak, R.H., Hassenstab, J., Snyder, P.J., Masters, C.L., Maruff, P., 2017. Cognitive impairment and decline in cognitively normal older adults with high amyloid-β: A meta-analysis. Alzheimer's & Dementia: Diagnosis, Assessment & Disease Monitoring 6 (1), 108–121. https://doi.org/10.1016/j.dadm.2016.09.002.

Berti, V., Walters, M., Sterling, J., Quinn, C.G., Logue, M., Andrews, R., Matthews, D.C., Osorio, R.S., Pupi, A., Vallabhajosula, S., Isaacson, R.S., de Leon, M.J., Mosconi, L., 2018. Mediterranean diet and 3-year Alzheimer brain biomarker changes in middle-aged adults. Neurology 90 (20), e1789–e1798.

Besson, F.L., La Joie, R., Doeuvre, L., Gaubert, M., Mezenge, F., Egret, S., Landeau, B., Barre, L., Abbas, A., Ibazizene, M., de La Sayette, V., Desgranges, B., Eustache, F., Chetelat, G., 2015. Cognitive and brain profiles associated with current neuroimaging biomarkers of preclinical Alzheimer's Disease. J. Neurosci. 35 (29), 10402–10411.

Blazhenets, G., Ma, Y., Sörensen, A., Rücker, G., Schiller, F., Eidelberg, D., Frings, L., Meyer, P.T., 2019. Principal components analysis of brain metabolism predicts development of alzheimer dementia. J. Nucl. Med. 60 (6), 837–843.

Bondi, M.W., Edmonds, E.C., Jak, A.J., Clark, L.R., Delano-Wood, L., McDonald, C.R., Nation, D.A., Libon, D.J., Au, R., Galasko, D., Salmon, D.P., 2014. Neuropsychological criteria for mild cognitive impairment improves diagnostic precision, biomarker associations, and progression rates. J. Alzheimers Dis. 42 (1), 275–289.

Chen, H., Sheng, X., Luo, C., Qin, R., Ye, Q., Zhao, H., Xu, Y., Bai, F., Alzheimer's Disease Neuroimaging Initiative, 2020. The compensatory phenomenon of the functional connectome related to pathological biomarkers in individuals with subjective cognitive decline. Translational neurodegeneration 9, 21. https://doi.org/10.1186/s40035-020-00201-6.

Dong, Q.Y., Li, T.R., Jiang, X.Y., Wang, X.N., Han, Y., Jiang, J.H., 2021. Glucose metabolism in the right middle temporal gyrus could be a potential biomarker for subjective cognitive decline: a study of a Han population. Alzheimers Res Ther 13, 74.

Du, W., Ding, C., Jiang, J., Han, Y., 2021. Women exhibit lower global left frontal cortex connectivity among cognitively unimpaired elderly individuals: a pilot study from SILCODE. Journal of Alzheimers Disease 83 (2), 653–663. https://doi.org/10.3233/JAD-210376.

Dubois, B., Epelbaum, S., Nyasse, F., Bakardjian, H., Gagliardi, G., Uspenskaya, O., Houot, M., Lista, S., Cacciamani, F., Potier, M.-C., Bertrand, A., Lamari, F., Benali, H., Mangin, J.-F., Colliot, O., Genthon, R., Habert, M.-O., Hampel, H., Audrain, C., Auffret, A., Baldacci, F., Benakki, I., Bertin, H., Boukadida, L., Cavedo, E., Chiesa, P., Dauphinot, L., Dos Santos, A., Dubois, M., Durrleman, S., Fontaine, G., Genin, A., Glasman, P., Jungalee, N., Kas, A., Kilani, M., La Corte, V., Lehericy, S., Letondor, C., Levy, M., Lowrey, M., Ly, J., Makiese, O., Metzinger, C., Michon, A., Mochel, F., Poisson, C., Ratovohery, S., Revillon, M., Rojkova, K., Roy, P., Santos-Andrade, K., Schindler, R., Seux, L., Simon, V., Sole, M., Tandetnik, C., Teichmann, M., Thiebaut de Shotten, M., Younsi, N., 2018. Cognitive and neuroimaging features and brain β-amyloidosis in individuals at risk of Alzheimer's disease (INSIGHT-preAD): a longitudinal observational study. Lancet Neurol. 17 (4), 335–346.

Dubois, B., Feldman, H.H., Jacova, C., Hampel, H., Molinuevo, José.L., Blennow, K., DeKosky, S.T., Gauthier, S., Selkoe, D., Bateman, R., Cappa, S., Crutch, S., Engelborghs, S., Frisoni, G.B., Fox, N.C., Galasko, D., Habert, M.-O., Jicha, G.A., Nordberg, A., Pasquier, F., Rabinovici, G., Robert, P., Rowe, C., Salloway, S., Sarazin, M., Epelbaum, S., de Souza, L.C., Vellas, B., Visser, P.J., Schneider, L., Stern, Y., Scheltens, P., Cummings, J.L., 2014. Advancing research diagnostic criteria for Alzheimer's disease: the IWG-2 criteria. Lancet Neurol. 13 (6), 614–629.

Dubois, B., Hampel, H., Feldman, H.H., Scheltens, P., Aisen, P., Andrieu, S., Bakardjian, H., Benali, H., Bertram, L., Blennow, K., Broich, K., Cavedo, E., Crutch, S., Dartigues, J., Duyckaerts, C., Epelbaum, S., Frisoni, G.B., Gauthier, S., Genthon, R., Gouw, A.A., Habert, M., Holtzman, D.M., Kivipelto, M., Lista, S., Molinuevo, J., O'Bryant, S.E., Rabinovici, G.D., Rowe, C., Salloway, S., Schneider, L. S., Sperling, R., Teichmann, M., Carrillo, M.C., Cummings, J., Jack, C.R., 2016. Preclinical Alzheimer's disease: Definition, natural history, and diagnostic criteria. Alzheimers Dement 12 (3), 292–323.

Eidelberg, D., 2009. Metabolic brain networks in neurodegenerative disorders: a functional imaging approach. Trends Neurosci. 32 (10), 548–557.

Eidelberg, D., Moeller, J.R., Dhawan, V., Spetsieris, P., Takikawa, S., Ishikawa, T., Chaly, T., Robeson, W., Margouleff, D., Przedborski, S., Fahn, S., 1994. The metabolic topography of parkinsonism. Journal of Cerebral Blood Flow and Metabolism 14 (5), 783–801. https://doi.org/10.1038/jcbfm.1994.99.

Eidelberg, D., Moeller, J.R., Ishikawa, T., Dhawan, V., Spetsieris, P., Przedborski, S., Fahn, S., 1995. The metabolic topography of idiopathic torsion dystonia. BRAIN 118 (Pt 6), 1473–1484. https://doi.org/10.1093/brain/118.6.1473.

Ewers, M., Brendel, M., Rizk-Jackson, A., Rominger, A., Bartenstein, P., Schuff, N., Weiner, M.W., 2014. Reduced FDG-PET brain metabolism and executive function predict clinical progression in elderly healthy subjects. Neuroimage Clin. 4, 45–52.

Fakhry-Darian, D., Patel, N.H., Khan, S., Barwick, T., Svensson, W., Khan, S., Perry, R.J., Malhotra, P., Carswell, C.J., Nijran, K.S., Win, Z., 2019. Optimisation and usefulness of quantitative analysis of 18F-florbetapir PET. Br. J. Radiol. 92 (1101), 20181020. https://doi.org/10.1259/bjr.20181020.

Golde, T.E., DeKosky, S.T., Galasko, D., 2018. Alzheimer's disease: The right drug, the right time. Science 362 (6420), 1250–1251.

Gonzalez-Escamilla, G., Lange, C., Teipel, S., Buchert, R., Grothe, M.J., 2017. Alzheimer's Disease Neuroimaging Initiative. PETPVE12: an SPM toolbox for Partial Volume Effects correction in brain PET - Application to amyloid imaging with AV45-PET. Neuroimage. 147, 669–677.

Gordon, B.A., Blazey, T.M., Su, Y., et al., 2018. Spatial patterns of neuroimaging biomarker change in individuals from families with autosomal dominant Alzheimer's disease: a longitudinal study. Lancet Neurol. 17 (3), 241–250.

Habeck, C., Foster, N.L., Perneczky, R., Kurz, A., Alexopoulos, P., Koeppe, R.A., Drzezga, A., Stern, Y., 2008. Multivariate and univariate neuroimaging biomarkers of Alzheimer's disease. Neuroimage. 40 (4), 1503–1515.

Hu, H., Chen, K.-L., Ou, Y.-N., Cao, X.-P., Chen, S.-D., Cui, M., Dong, Q., Tan, L., Yu, J.-T., 2019. Neurofilament light chain plasma concentration predicts neurodegeneration and clinical progression in nondemented elderly adults. Aging (Albany NY). 11 (17), 6904–6914.

Jack, C.R., Bennett, D.A., Blennow, K., Carrillo, M.C., Dunn, B., Haeberlein, S.B., Holtzman, D.M., Jagust, W., Jessen, F., Karlawish, J., Liu, E., Molinuevo, J.L., Montine, T., Phelps, C., Rankin, K.P., Rowe, C.C., Scheltens, P., Siemers, E., Snyder, H.M., Sperling, R., Elliott, C., Masliah, E., Ryan, L., Silverberg, N., 2018. NIA-AA Research Framework: Toward a biological definition of Alzheimer's disease. Alzheimers Dement. 14 (4), 535–562.

Jagust, W.J., Landau, S.M., 2012. Alzheimer's Disease Neuroimaging Initiative. Apolipoprotein E, not fibrillar β-amyloid, reduces cerebral glucose metabolism in normal aging. J. Neurosci. 32, 18227–18233.

Johnson, S.C., Christian, B.T., Okonkwo, O.C., Oh, J.M., Harding, S., Xu, G., Hillmer, A. T., Wooten, D.W., Murali, D., Barnhart, T.E., Hall, L.T., Racine, A.M., Klunk, W.E., Mathis, C.A., Bendlin, B.B., Gallagher, C.L., Carlsson, C.M., Rowley, H.A., Hermann, B.P., Dowling, N.M., Asthana, S., Sager, M.A., 2014. Amyloid burden and neural function in people at risk for Alzheimer's Disease. Neurobiol. Aging 35 (3), 576–584.

Kadir, A., Almkvist, O., Forsberg, A., Wall, A., Engler, H., Långström, B., Nordberg, A., 2012. Dynamic changes in PET amyloid and FDG imaging at different stages of Alzheimer's disease. Neurobiol. Aging 33 (1), 198.e1–198.e14.

Katako, A., Shelton, P., Goertzen, A.L., Levin, D., Bybel, B., Aljuaid, M., Yoon, H.J., Kang, D.Y., Kim, S.M., Lee, C.S., Ko, J.H., 2018. Machine learning identified an Alzheimer's disease-related FDG-PET pattern which is also expressed in Lewy body dementia and Parkinson's disease dementia. Sci. Rep. 8 (1) https://doi.org/10.1038/s41598-018-31653-6.

Kato, T., Inui, Y., Nakamura, A., Ito, K., 2016. Brain fluorodeoxyglucose (FDG) PET in dementia. Ageing Res Rev. 30, 73–84.

Knopman, D.S., Jack, C.R., Wiste, H.J., Weigand, S.D., Vemuri, P., Lowe, V.J., Kantarci, K., Gunter, J.L., Senjem, M.L., Mielke, M.M., Roberts, R.O., Boeve, B.F., Petersen, R.C., 2013. Selective worsening of brain injury biomarker abnormalities in cognitively normal elderly persons with β-amyloidosis. JAMA Neurol. 70 (8), 1030. https://doi.org/10.1001/jamaneurol.2013.182.

Lammertsma, A.A., 2017. Forward to the Past: The Case for Quantitative PET Imaging. J. Nucl. Med. 58 (7), 1019–1024.

Landau, S.M., Harvey, D., Madison, C.M., Koeppe, R.A., Reiman, E.M., Foster, N.L., Weiner, M.W., Jagust, W.J., Initiative, A.D.N., 2011. Associations between cognitive, functional, and FDG-PET measures of decline in AD and MCI. Neurobiol. Aging 32, 1207–1218. https://doi.org/10.1016/j.neurobiolaging.2009.07.002.

Li, T.-R., Wu, Y., Jiang, J.-J., Lin, H., Han, C.-L., Jiang, J.-H., Han, Y., 2020. Radiomics analysis of magnetic resonance imaging facilitates the identification of preclinical Alzheimer's Disease: an exploratory study. Front. Cell Dev. Biol. 8, 605734.

Li, T.-R., Yang, Q., Hu, X., Han, Y., 2021. Biomarkers and Tools for Predicting Alzheimer's Disease at the Preclinical Stage. Curr. Neuropharmacol. 19 https://doi.org/10.2174/1570159X19666210524153901.

Li, X., Wang, X., Su, L., Hu, X., Han, Y., 2019. Sino Longitudinal Study on Cognitive Decline (SILCODE): protocol for a Chinese longitudinal observational study to develop risk prediction models of conversion to mild cognitive impairment in individuals with subjective cognitive decline. BMJ Open. 9 (7), e028188. https://doi.org/10.1136/bmjopen-2018-028188.

Long, J.M., Holtzman, D.M., 2019. Alzheimer Disease: An Update on Pathobiology and Treatment Strategies. Cell 179 (2), 312–339.

Luo, J., Agboola, F., Grant, E., Masters, C.L., Albert, M.S., Johnson, S.C., McDade, E.M., Vöglein, J., Fagan, A.M., Benzinger, T., Massoumzadeh, P., Hassenstab, J., Bateman, R.J., Morris, J.C., Perrin, R.J., Chhatwal, J., Jucker, M., Ghetti, B., Cruchaga, C., Graff-Radford, N.R., Schofield, P.R., Mori, H., Xiong, C., 2020. Sequence of Alzheimer disease biomarker changes in cognitively normal adults: A cross-sectional study. Neurology. 95 (23), e3104–e3116.

Matthews, D.C., Davies, M., Murray, J., Williams, S., Tsui, W.H., Li, Y., Andrews, R.D., Lukic, A., McHugh, P., Vallabhajosula, S., de Leon, M.J., Mosconi, L., 2014. Physical Activity, Mediterranean Diet and Biomarkers-Assessed Risk of Alzheimer's: A Multi-Modality Brain Imaging Study. Adv J Mol Imaging 04 (04), 43–57.

Mattis, P.J., Niethammer, M., Sako, W., Tang, C.C., Nazem, A., Gordon, M.L., Brandt, V., Dhawan, V., Eidelberg, D., 2016. Distinct brain networks underlie cognitive dysfunction in Parkinson and Alzheimer diseases. Neurology. 87 (18), 1925–1933.

McKhann, G., Drachman, D., Folstein, M., Katzman, R., Price, D., Stadlan, E.M., 1984. Clinical diagnosis of Alzheimer's disease: report of the NINCDS-ADRDA Work Group under the auspices of Department of Health and Human Services Task Force on Alzheimer's Disease. Neurology. 34 (7), 939.

McKhann, G.M., Knopman, D.S., Chertkow, H., Hyman, B.T., Jack, C.R., Kawas, C.H., Klunk, W.E., Koroshetz, W.J., Manly, J.J., Mayeux, R., Mohs, R.C., Morris, J.C., Rossor, M.N., Scheltens, P., Carrillo, M.C., Thies, B., Weintraub, S., Phelps, C.H., 2011. The diagnosis of dementia due to Alzheimer's disease: recommendations from the National Institute on Aging-Alzheimer's Association workgroups on diagnostic guidelines for Alzheimer's disease. Alzheimers Dement. 7 (3), 263–269.

Meles, S.K., Kok, J.G., De Jong, B.M., Renken, R.J., de Vries, J.J., Spikman, J.M., Ziengs, A.L., Willemsen, A.T.M., van der Horn, H.J., Leenders, K.L., Kremer, H.P.H., 2018. The cerebral metabolic topography of spinocerebellar ataxia type 3. Neuroimage Clin 19, 90–97.

Meles, S.K., Pagani, M., Arnaldi, D., De Carli, F., Dessi, B., Morbelli, S., Sambuceti, G., Jonsson, C., Leenders, K.L., Nobili, F., 2017. The Alzheimer's disease metabolic brain pattern in mild cognitive impairment. J. Cereb. Blood Flow Metab. 37 (12), 3643–3648.

Moeller, J.R., Ishikawa, T., Dhawan, V., Spetsieris, P., Mandel, F., Alexander, G.E., Grady, C., Pietrini, P., Eidelberg, D., 1996. The metabolic topography of normal aging. Journal of Cerebral Blood flow and Metabolism 16 (3), 385–398. https://doi.org/10.1097/00004647-199605000-00005.

Morbelli, S., Brugnolo, A., Bossert, I., Buschiazzo, A., Frisoni, G.B., Galluzzi, S., van Berckel, B.N.M., Ossenkoppele, R., Perneczky, R., Drzezga, A., Didic, M., Guedj, E., Sambuceti, G., Bottoni, G., Arnaldi, D., Picco, A., De Carli, F., Pagani, M., Nobili, F., 2015. Visual versus semi-quantitative analysis of 18F-FDG-PET in amnestic MCI: an European Alzheimer's Disease Consortium (EADC) project. J. Alzheimers Dis. 44 (3), 815–826.

Oh, H., Habeck, C., Madison, C., Jagust, W., 2014. Covarying alterations in Aβ deposition, glucose metabolism, and gray matter volume in cognitively normal elderly. Hum. Brain Mapp. 35 (1), 297–308.

Sakamoto, S., Ishii, K., Sasaki, M., Hosaka, K., Mori, T., Matsui, M., Hirono, N., Mori, E., 2002. Differences in cerebral metabolic impairment between early and late onset types of Alzheimer's disease. J. Neurol. Sci. 200 (1-2), 27–32.

Seo, E.H., Kim, S.H., Park, S.H., Kang, S.-H., Choo, IL.H., Lee, J.-Y., 2016. Topographical APOE ε4 genotype influence on cerebral metabolism in the continuum of Alzheimer's Disease: amyloid burden adjusted analysis. Journal of Alzheimers Disease 54 (2), 559–568. https://doi.org/10.3233/JAD-160395.

Shaw, L.M., Vanderstichele, H., Knapik-Czajka, M., Clark, C.M., Aisen, P.S., Petersen, R. C., Blennow, K., Soares, H., Simon, A., Lewczuk, P., Dean, R., Siemers, E., Potter, W., Lee, V.-Y., Trojanowski, J.Q., 2009. Cerebrospinal fluid biomarker signature in Alzheimer's disease neuroimaging initiative subjects. Ann. Neurol. 65 (4), 403–413. https://doi.org/10.1002/(ISSN)1531-824910.1002/ana.v65:410.1002/ana.21610.

Shen, X., Liu, H., Hu, Z., Hu, H., Shi, P., Fan, Y., 2012. The relationship between cerebral glucose metabolism and age: report of a large brain PET data set. PLoS ONE 7 (12), e51517.

Skouras, S., Falcon, C., Tucholka, A., Rami, L., Sanchez-Valle, R., Lladó, A., Gispert, J.D., Molinuevo, José.Luís., 2019. Mechanisms of functional compensation, delineated by eigenvector centrality mapping, across the pathophysiological continuum of Alzheimer's disease. NeuroImage-Clinical 22, 101777. https://doi.org/10.1016/j.nicl.2019.101777.

Spetsieris, P.G., Ma, Y., Eckert, T., Dhawan, V., Eidelberg, D., 2007. New strategies for automated differential diagnosis of degenerative brain disorders. Annual International Conference of the IEEE Engineering in Medicine and Biology Society 2007, 3421–3425. https://doi.org/10.1109/IEMBS.2007.4353066.

Spetsieris, P.G., Eidelberg, D., 2011. Scaled subprofile modeling of resting state imaging data in Parkinson's disease: methodological issues. Neuroimage. 54 (4), 2899–2914.

Stonnington, C.M., Chen, Y., Savage, C.R., Lee, W., Bauer III, R.J., Sharieff, S., Thiyyagura, P., Alexander, G.E., Caselli, R.J., Locke, D.E.C., Reiman, E.M., Chen, K., Bendlin, B., 2018. Predicting Imminent Progression to Clinically Significant Memory Decline Using Volumetric MRI and FDG PET. J. Alzheimers Dis. 63 (2), 603–615.

Stonnington, C.M., Velgos, S.N., Chen, Y., Syed, S., Huentelman, M., Thiyyagura, P., Lee, W., Richholt, R., Caselli, R.J., Locke, D.E.C., Lu, B., Reiman, E.M., Su, Y., Chen, K., 2020. Interaction Between BDNF Val66Met and APOE4 on Biomarkers of Alzheimer's Disease and Cognitive Decline. J. Alzheimers Dis. 78 (2), 721–734.

Sun, Y., Dai, Z., Li, Y., Sheng, C., Li, H., Wang, X., Chen, X., He, Y., Han, Y., 2016. Subjective Cognitive Decline: Mapping Functional and Structural Brain Changes-A Combined Resting-State Functional and Structural MR Imaging Study. Radiology 281 (1), 185–192. https://doi.org/10.1148/radiol.2016151771.

Teune, L.K., Renken, R.J., Mudali, D., De Jong, B.M., Dierckx, R.A., Roerdink, J.B.T.M., Leenders, K.L., 2013. Validation of parkinsonian disease-related metabolic brain patterns. Mov. Disord. 28 (4), 547–551.

Teune, L.K., Strijkert, F., Renken, R.J., et al., 2014. The Alzheimer's disease-related glucose metabolic brain pattern. Curr. Alzheimer Res. 11 (8), 725–732.

Toledo, J.B., Weiner, M.W., Wolk, D.A., Da, X., Chen, K., Arnold, S.E., Jagust, W., Jack, C., Reiman, E.M., Davatzikos, C., Shaw, L.M., Trojanowski, J.Q., 2014. Neuronal injury biomarkers and prognosis in ADNI subjects with normal cognition. Acta Neuropathol Commun 2 (1). https://doi.org/10.1186/2051-5960-2-26.

Verberk, I.M.W., Teunissen, C.E., Van der Flier, W.M., 2020. Reply to "Usefulness of Plasma Amyloid as Prescreener of the Earliest Alzheimer Pathological Changes Depends on the Study Population". Ann. Neurol. 87 (1), 155.

Wolfsgruber, S., Kleineidam, L., Guski, J., Polcher, A., Frommann, I., Roeske, S., Spruth, E.J., Franke, C., Priller, J., Kilimann, I., Teipel, S., Buerger, K., Janowitz, D., Laske, C., Buchmann, M., Peters, O., Menne, F., Fuentes Casan, M., Wiltfang, J., Bartels, C., Düzel, E., Metzger, C., Glanz, W., Thelen, M., Spottke, A., Ramirez, A., Kofler, B., Fließbach, K., Schneider, A., Heneka, M.T., Brosseron, F., Meiberth, D., Jessen, F., Wagner, M., DELCODE Study Group, 2020. Minor neuropsychological deficits in patients with subjective cognitive decline. NEUROLOGY 95, e1134-1134e1143. https://doi.org/10.1212/WNL.0000000000010142.

Yang, L., Yan, Y., Wang, Y., Hu, X., Lu, J., Chan, P., Yan, T., Han, Y., 2018. Gradual Disturbances of the Amplitude of Low-Frequency Fluctuations (ALFF) and Fractional ALFF in Alzheimer Spectrum. Front. Neurosci. 12, 975. https://doi.org/10.3389/fnins.2018.00975.

Zhang, C., Kong, M., Wei, H., Zhang, H., Ma, G., Ba, M., Alzheimer's Disease Neuroimaging Initiative, 2020. The effect of ApoE ε 4 on clinical and structural MRI markers in prodromal Alzheimer's disease. Quantitative imaging in medicine and surgery 10, 464-474. https://doi.org/10.21037/qims.2020.01.14.